Dynamic analysis and fractional-order adaptive sliding mode control for a novel fractional-order ferroresonance system*

Ningning Yang(杨宁宁)[1,2], Yuchao Han(韩宇超)[2], Chaojun Wu(吴朝俊)[3,†], Rong Jia(贾嵘)[1,2], and Chongxin Liu(刘崇新)[4]

[1] *State Key Laboratory Base of Eco-hydraulic Engineering in Arid Area, Xi'an University of Technology, Xi'an* 710048, *China*
[2] *Institute of Water Resources and Hydro-electric Engineering, Xi'an University of Technology, Xi'an* 710048, *China*
[3] *College of Electronics and Information, Xi'an Polytechnic University, Xi'an* 710048, *China*
[4] *School of Electrical Engineering, Xi'an Jiaotong University, Xi'an* 710049, *China*

(Received 15 February 2017; revised manuscript received 19 April 2017; published online 10 July 2017)

Ferroresonance is a complex nonlinear electrotechnical phenomenon, which can result in thermal and electrical stresses on the electric power system equipments due to the over voltages and over currents it generates. The prediction or determination of ferroresonance depends mainly on the accuracy of the model used. Fractional-order models are more accurate than the integer-order models. In this paper, a fractional-order ferroresonance model is proposed. The influence of the order on the dynamic behaviors of this fractional-order system under different parameters n and F is investigated. Compared with the integral-order ferroresonance system, small change of the order not only affects the dynamic behavior of the system, but also significantly affects the harmonic components of the system. Then the fractional-order ferroresonance system is implemented by nonlinear circuit emulator. Finally, a fractional-order adaptive sliding mode control (FASMC) method is used to eliminate the abnormal operation state of power system. Since the introduction of the fractional-order sliding mode surface and the adaptive factor, the robustness and disturbance rejection of the controlled system are enhanced. Numerical simulation results demonstrate that the proposed FASMC controller works well for suppression of ferroresonance over voltage.

Keywords: fractional-order ferroresonance system, fractional-order sliding mode control, adaptive control, nonlinear circuit emulator

PACS: 05.45.–a, 05.45.Gg, 05.45.Pq **DOI:** 10.1088/1674-1056/26/8/080503

1. Introduction

Fractional calculus, as a mathematical problem with a long history, plays a very important role in various fields of science and engineering. It has been accepted as a novel modeling method which can extend the descriptive power of the conventional calculus, yield a more accurate description and give a deeper insight into the physical processes underlying a long range memory behaviour.[1–4] New researches suggest that many real objects are "intrinsic" fractional-order, such as real capacitors and inductors. In Ref. [5], Jonscher and his partner pointed out that there are no ideal integer-order capacitors in nature, capacitors are all fractional-order components.[5] Westerlund and his partner established the fractional-order model of the capacitor, and measured the orders of fractional-order capacitors in different dielectrics experimentally.[6] Jesus and his partners realized fractional-order capacitors with different orders.[7] Haba and his partner created the fractional-order capacitor.[8] Many real dynamical circuits, like fractional-order Chua's system, viscoelasticity model, nonlocal epidemics model, and so on, were better characterized by non-integer order models based on fractional calculus.[9–17]

Ferroresonance as a complex nonlinear electrotechnical phenomenon has been studied over the past 100 years and is nowadays well established among electrical engineers.[18–20] The predictive power of ferroresonance depends mainly on the accuracy and fidelity of the model used. Because of its accuracy and flexibility, the fractional-order model accords with the requirement of the ferroresonance system modeling. Since the intrinsic fractional-order behavior of real capacitors and inductors, the idea of establishing the fractional-order model of ferroresonance seems to be far more sensible. The introduction of the order which can be seen as an adjustable parameter of the model, the degrees of freedom and flexibility of the model are increased. As far as the author is concerned, there are few studies on fractional-order ferroresonance.

In recent years the number of ferroresonance incidents has increased due to network complexity and improved equipment efficiency.[21,22] There are many unknown parameters and disturbances in the actual operation of power system. The suppression of ferroresonance has become a hot issue for scholars. The combination of fractional calculus and control theory has attracted more and more attention. Twenty

*Project supported by the National Natural Science Foundation of China (Grant No. 51507134) and the Science Fund from the Education Department of Shaanxi Province, China (Grant No. 15JK1537).

†Corresponding author. E-mail: chaojun.wu@stu.xjtu.edu.cn

© 2017 Chinese Physical Society and IOP Publishing Ltd

years ago, Oustaloup and partners proposed the first fractional-order controller CRONE.[23] Then a variety of fractional-order control methods have been proposed, such as fractional-order PID control,[24] fractional-order sliding mode control,[25,26] fractional-order optimal control,[27] etc. Sliding mode control (SMC) is an effective robust control strategy. When in the sliding mode, the closed loop response becomes totally insensitive to both internal parameter uncertainties and external disturbances.[28–30] Combining the fractional calculus with sliding mode control, the fractional-order sliding mode control strategy is more robust and of better features than conventional SMC.[31,32]

In this paper, based on the fractional calculus theory, a ferroresonance system is extended to fractional-order system. And an adaptive sliding mode control with fractional-order sliding surface is proposed. The rest of this paper is organized as follows: In Section 2, firstly, fractional calculus theory is introduced briefly. Then a fractional-order ferroresonance system model is established. The influence of the order on the dynamic behavior of ferroresonance system and the dynamic behaviors of this fractional-order system under different parameters n and F are investigated. In Section 3, the fractional-order ferroresonance system is implemented by nonlinear circuit emulator. In Section 4, an adaptive sliding mode controller with fractional-order sliding surface is proposed to eliminate the abnormal operation state of power system. Finally, the conclusion part summarizes the whole development process and presents some concluding remarks.

2. Modeling and analysis of ferroresonance system based on fractional calculus

2.1. Fractional calculus

The theory and applications of fractional calculus had a considerable progress during the last two decades. Researchers have reported the "intrinsic" fractional-order behavior of real objects. And it has been demonstrated that fractional-order models can increase the flexibility and degrees of freedom by means of fractional-order parameters.[1,2] The fundamental operator: ${}_aD_t^\alpha$ is defined as

$$ {}_aD_t^\alpha = \begin{cases} \dfrac{\mathrm{d}^\alpha}{\mathrm{d}t^\alpha}, & \alpha > 0, \\ 1, & \alpha = 0, \\ \int_a^t (\mathrm{d}\tau)^{-\alpha}, & \alpha < 0, \end{cases} \tag{1} $$

where $\alpha\,(\alpha \in R)$ is the order, a and t are the bounds of the operation.

There are three best known definitions for fractional calculus: Grünwald–Letnikov (GL) definition, Riemann–Liouville (RL) definition, and Caputo definition.

Caputo definition is more convenient for initial conditions problems, so in this paper, it is used. The fractional derivative of $f(t)$ is defined as

$$ {}_aD_t^\alpha f(t) = \frac{1}{\Gamma(n-\alpha)} \int_a^t \frac{f^{(n)}(\tau)}{(t-\tau)^{\alpha-n+1}} \mathrm{d}\tau, \tag{2} $$

where $\Gamma(\cdot)$ is the Gamma function, and $n \in N$ is the first integer which is not less than α, $n-1 < \alpha < n$.

The Laplace transform of Caputo fractional derivative satisfies

$$ \begin{aligned} &L\{{}_aD_t^\alpha f(t)\} \\ &= s^\alpha F(s) - \sum_{k=0}^{n-1} s^{\alpha-k-1} f^{(k)}(0), \quad n-1 < \alpha < n. \end{aligned} \tag{3} $$

For zero initial conditions, the Laplace transform of fractional derivatives has the form

$$ L\{{}_aD_t^\alpha f(t)\} = s^\alpha F(s). \tag{4} $$

2.2. Analysis of integer-order ferroresonance system

Ferroresonance is an effective term between power system engineers and can be applied to a wide variety of capacitors and nonlinear inductors. In this paper, a single phase iron core transformer circuit which is three-order non-autonomous ferroresonance chaotic circuit, as shown in Fig. 1, is selected as the research object.[20] N_2 is the primary side of the iron core transformer. N_1 is the secondary side. The circuit is drived by a sinusoidal voltage source. The current through the resistance, capacitance, and inductance, respectively.

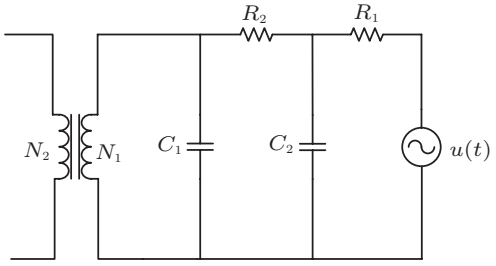


Fig. 1. Ferroresonance circuit of a single phase transformer.

Transformer magnetization characteristics is approximated by polynomial expression $i_3 = a\psi^n + b\psi$, where ψ donates the flux in the nonlinear inductance, n is the index of nonlinearity of the curve. With the excitation of the sinusoidal power source $u(t) = U_m \sin(\omega t)$, when the transformer coil is saturated, the inductor coil is regarded as the nonlinear inductance element. the system model is:

$$ \begin{aligned} &\frac{\mathrm{d}\psi}{\mathrm{d}t} = u_{c1}, \\ &C_1 \frac{\mathrm{d}u_{c1}}{\mathrm{d}t} = \frac{u_{c2}-u_{c1}}{R_2} - (a\psi^n + b\psi), \\ &C_2 \frac{\mathrm{d}u_{c2}}{\mathrm{d}t} = \frac{u(t)-u_{c2}}{R_1} - \frac{u_{c2}-u_{c1}}{R_2}. \end{aligned} \tag{5} $$

Set $x_1 = \psi$, $x_2 = u_{c1}/\omega$, $x_3 = u_{c2}/\omega$, $\tau = \omega t$, the equation can be written as follows:

$$\begin{aligned} \frac{\mathrm{d}x_1}{\mathrm{d}\tau} &= x_2, \\ \frac{\mathrm{d}x_2}{\mathrm{d}\tau} &= \alpha\left(x_3 - x_2\right) - \zeta\left(a x_1^n + b x_1\right), \\ \frac{\mathrm{d}x_3}{\mathrm{d}\tau} &= \beta\left(x_2 - x_3\right) - \eta x_3 + F\sin\tau, \end{aligned} \tag{6}$$

where $F = U_m/(\omega^2 C_2 R_1)$, $\alpha = 1/(\omega C_1 R_2)$, $\beta = 1/(\omega C_2 R_2)$, $\zeta = 1/(\omega^2 C_1)$, $\eta = 1/(\omega C_2 R_1)$.

When the outside source $F\sin\tau = 0$, $R_1 = 163.3\ \Omega$, $R_2 = 816.6\ \Omega$, $C_1 = 15.6\ \mu\mathrm{F}$, $C_2 = 30\ \mu\mathrm{F}$, $a = 1$, $b = 1$, the system become a three-order autonomous circuit. The equilibrium point is $O(0,0,0)$, the Jacobian matrix is

$$J = \begin{pmatrix} 0 & 1 & 0 \\ -0.65\left(n x^{n-1} + 1\right) & -0.25 & 0.25 \\ 0 & 0.13 & -0.78 \end{pmatrix}. \tag{7}$$

When $n = 3$, characteristic roots of the system are $\lambda_1 = -0.1131 + \mathrm{j}0.7861$, $\lambda_2 = -0.1131 - \mathrm{j}0.7861$, $\lambda_3 = -0.8039$. λ_1 and λ_2 are a pair of the conjugate complex roots with negative real part, λ_3 is a negative real root, so the equilibrium point O is stable. When the external excitation is not zero, the three-order nonlinear non-autonomous system can enter into the chaotic state.

As shown in Fig. 2(a), when $F = 1$, the magnitude of external excitation is small, due to the normalization process, the fundamental frequency of the system is 0.1579. When $F = 260$, the harmonic components become complex. The fundamental component is no longer the main component. As shown in Figs. 2(b) and 2(c), when $F = 1$, the system is actually stable. When $F = 260$, the system is chaos. The amplitude of the state variable x_2 increases significantly. It means that the system is over voltage. Poincare sections also verifies that the dynamic behavior of the system varies with the parameter as shown in Fig. 2(d).

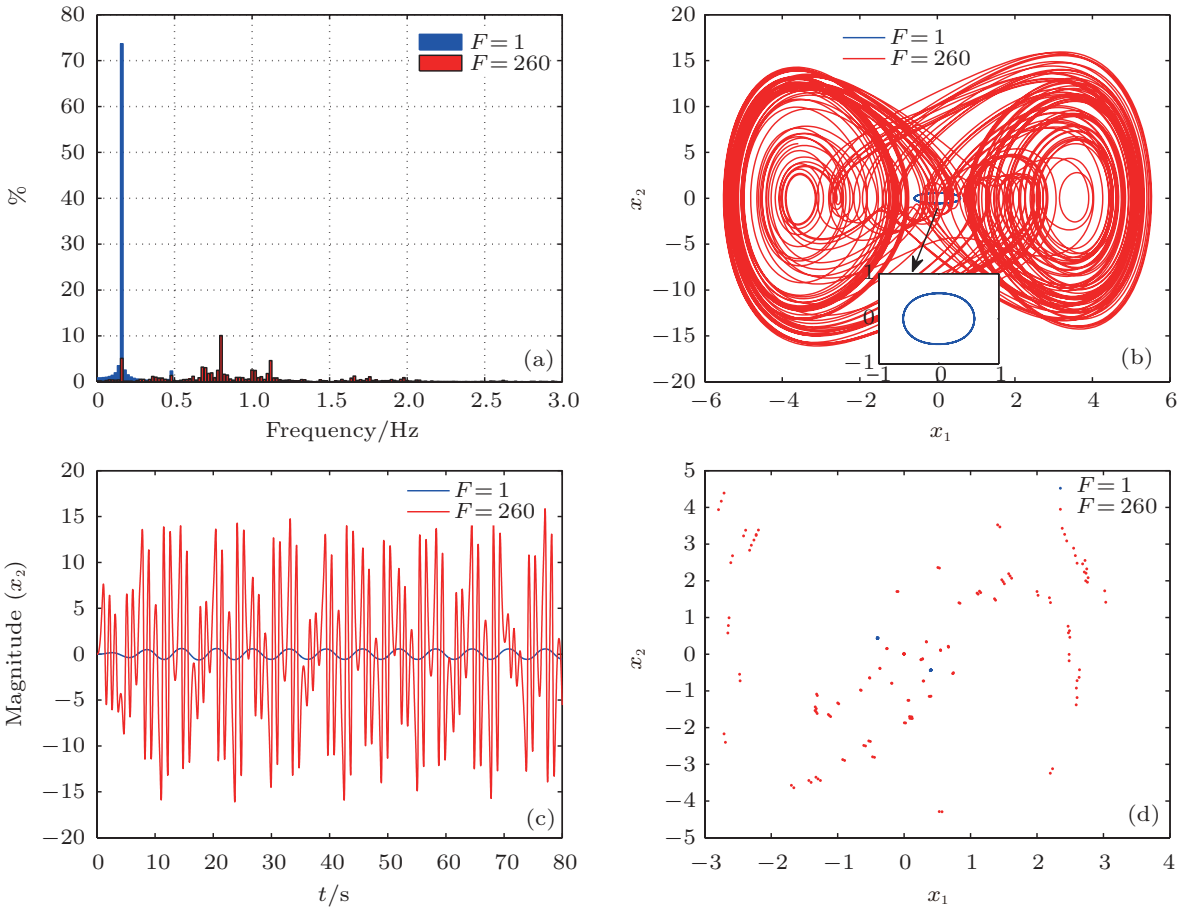


Fig. 2. (color online) Dynamic behavior analysis of ferroresonance system with the variation of parameters. (a) Harmonic spectrum, (b) phase plane orbit, (c) waveform plane, and (d) Poincare section on $x_3 = 0$.

In Fig. 3, when $F = 260$, one Lyapunov exponent is positive, the system is in chaotic state.

With the increase of the index of nonlinearity n, the current through iron core transformer is increased dramatically as shown in Fig. 4. The Lyapunov exponent in Fig. 5(a)–5(d) reveal that with the increase of n, the amplitude of the external excitation F which drive the system enter into chaos is reduced. The chaotic region of parameter F becomes larger.

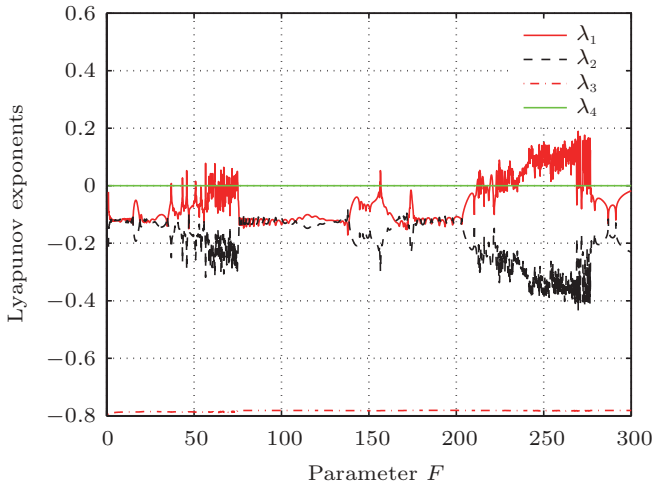


Fig. 3. (color online) The Lyapunov exponent for $n = 3$.

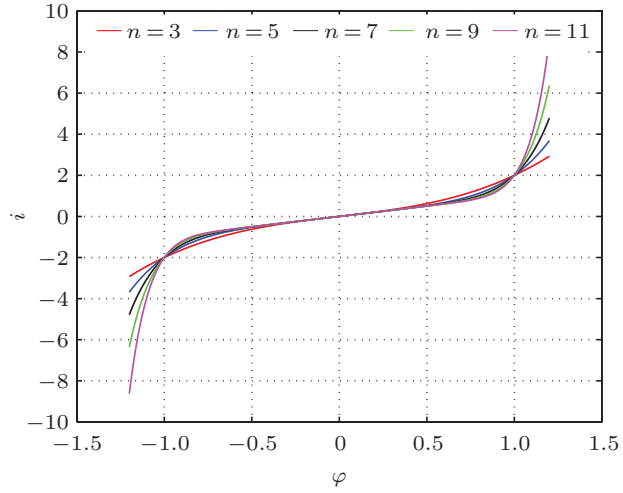


Fig. 4. (color online) Index of nonlinearity of the curve.

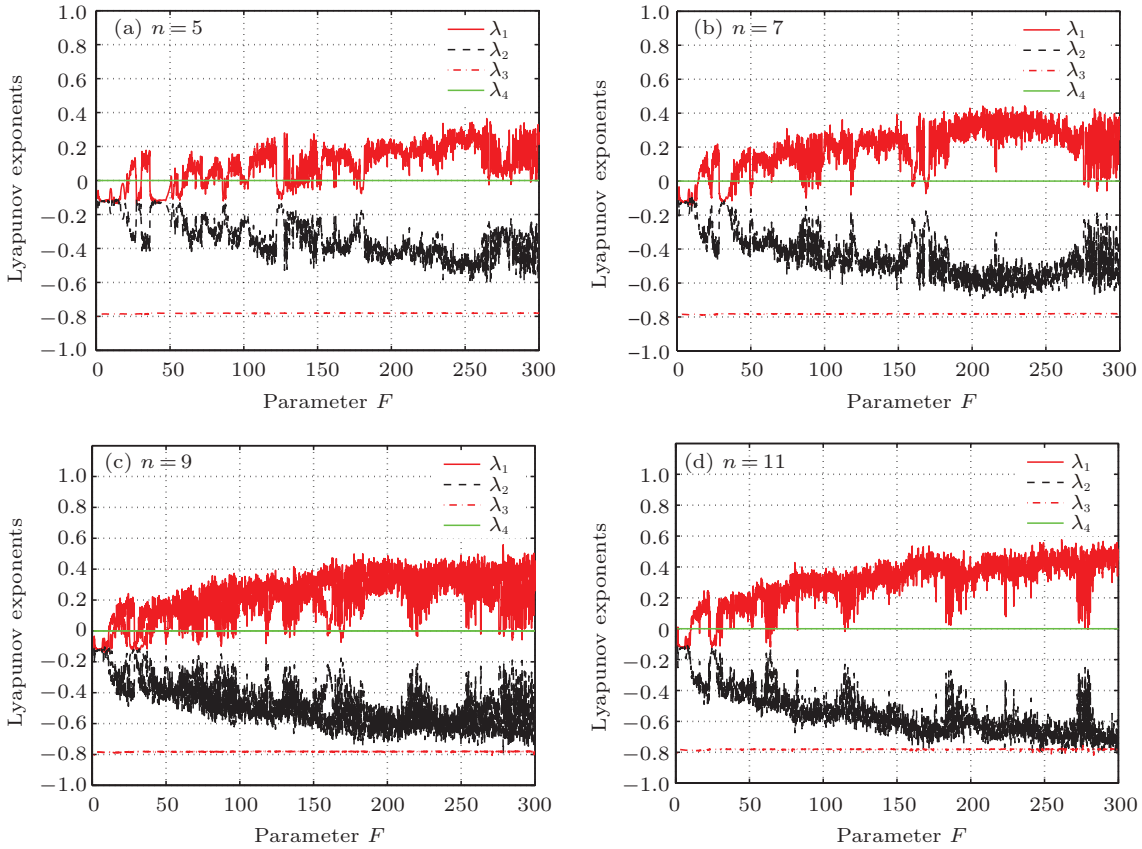


Fig. 5. (color online) The Lyapunov exponent of chaotic system.

2.3. Modeling and analysis of fractional-order ferroresonance system

At present a large number of researches indicate that the actual inductance and capacitance are all fractional-order.[33,34] The fractional-order model is more accurate than the integer-order model, and the flexibility and freedom of the system are increased due to the introduction of the order parameter. However, due to the limitation of the analytical methods and the implementation methods, ferroresonance systems are currently integer-order models.

The model of the iron core transformer is formed with two capacitances C_1 and C_2 which can be written as fractional-order model. That means two of the three differential equations is fractional-order which makes the system less than 3 order. Consider the fractional-order form of the ferroresonance system (6), the standard derivative is replaced by a fractional derivative as follows:

$$\frac{\mathrm{d}x_1}{\mathrm{d}\tau} = x_2,$$
$$\frac{\mathrm{d}^q x_2}{\mathrm{d}\tau^q} = \alpha\left(x_3 - x_2\right) - \zeta\left(a x_1^n + b x_1\right),$$

$$\frac{\mathrm{d}^q x_3}{\mathrm{d}\tau^q} = \beta(x_2 - x_3) - \eta x_3 + F\sin\tau. \tag{8}$$

Adams–Bashforth–Moulton method proposed by Diethelm is adopted in this paper.[35] Predictor corrector algorithm is the main method to solve fractional-order nonlinear system in the time domain, this method has the advantages of calculating the differential operator with arbitrary order.

As shown in Fig. 6 and Fig. 7, set the order $q = 0.99$ and F is changed from 0 to 1000, the periodic and chaotic states of the system appear alternately. When $F < 61$, the system is in the periodic state. When $F = 300$, the system is in chaotic state as shown in Fig. 6(c), the fractional-order chaotic attractor is similar to the integer-order one. When the parameter F ranging from 350 to 650, the system becomes periodic.

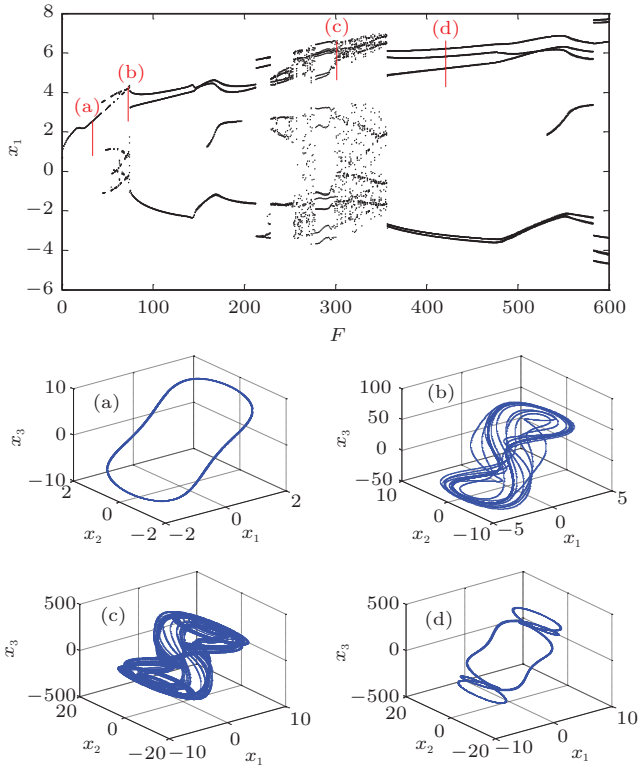


Fig. 6. (color online) Bifurcation diagram of the order of 0.99 (1–600).

The system is turning into a state of chaos by period doubling bifurcation. The chaotic strange attractor is a product of global stability and local instability, and the performance of the orbit in phase space is the extension and folding. So they are neither balanced nor divergent in phase space, unlimited filling and loitering in space.

External excitation F takes the following different values: $F = 61, 250, 800, 1000$, simulation results using these parameter F which is choosing from different areas in bifurcation diagram contain different states, such as chaos and periodic states. Phase diagrams and the corresponding time-domain waveform are shown in Fig. 8. It indicates that the trajectory has changed from limit cycles to chaotic strange attractors. But when $F = 1000$, the voltage of this model becomes periodic state after a short transient process while the maximum over-voltage becomes smaller.

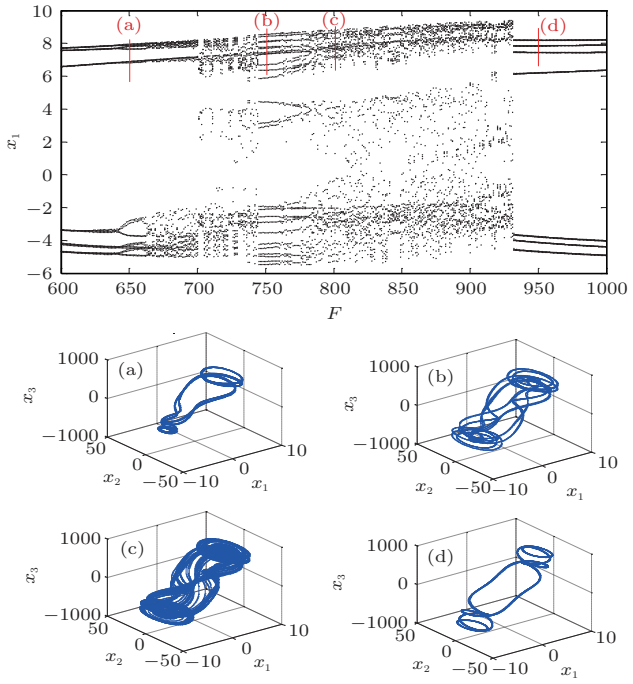


Fig. 7. (color online) Bifurcation diagram of the order of 0.99 (600–1000).

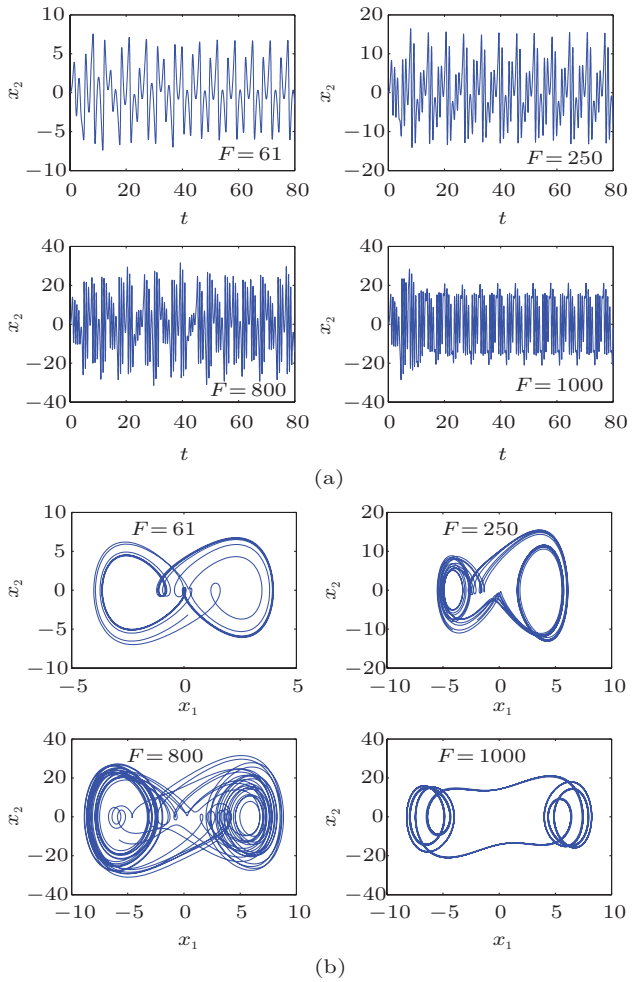


Fig. 8. (color online) Waveform plane orbit of $F = 61, 250, 800, 1000$. (a) Time-domain waveform. (b) Phase diagram.

In order to study the influence of order on the dynamic behavior of the system, reduce the order to 0.95, dynamic behaviors of the system changed significantly,as shown in Figs. 9, 10, 11, 12, and 13.

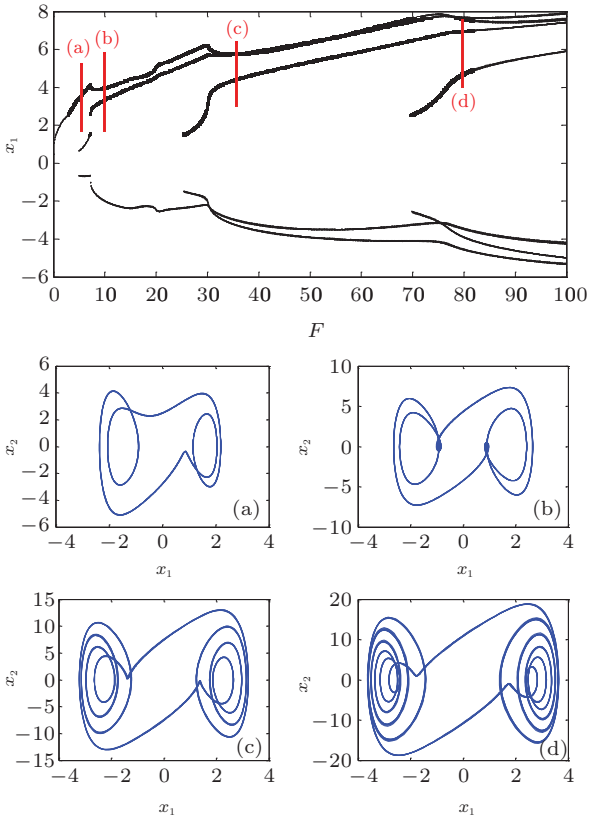


Fig. 9. (color online) Bifurcation diagram of the order of 0.95 for $n = 3$.

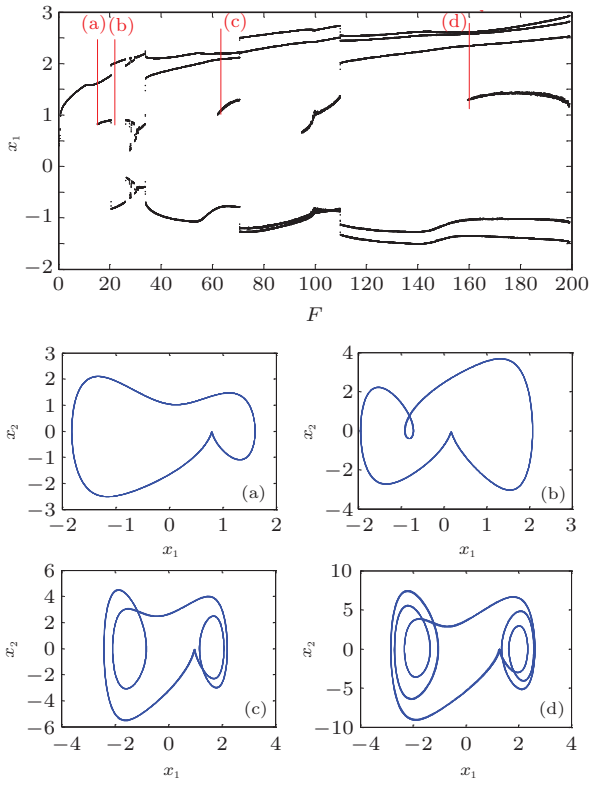


Fig. 10. (color online) Bifurcation diagram of the order of 0.95 when $n = 5$.

There are no chaotic states in this system for $n = 3$ and $n = 5$. The waveform of x_1 is still periodic state as shown in Fig. 9 and Fig. 10. The trajectory in phase diagram stay in limit cycle all the time. It indicates that the fractional-order ferroresonance is hardly happened.

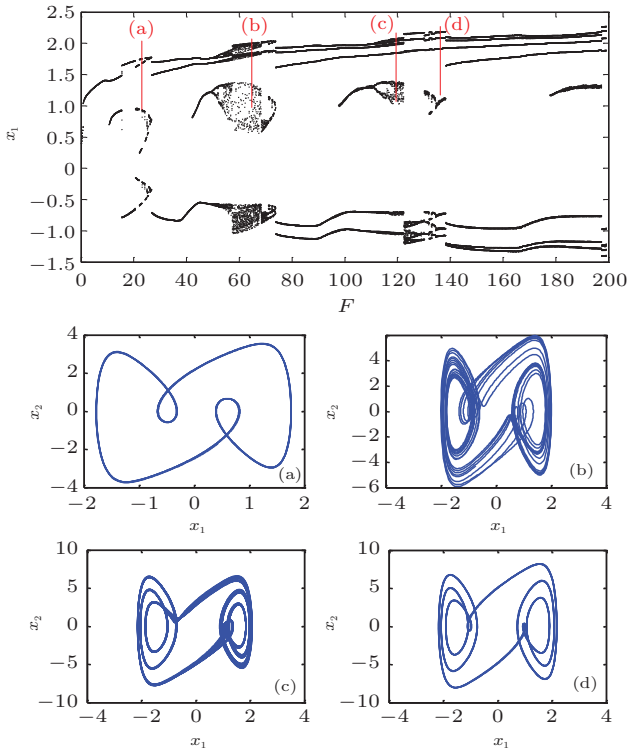


Fig. 11. (color online) Bifurcation diagram of the order of 0.95 when $n = 7$.

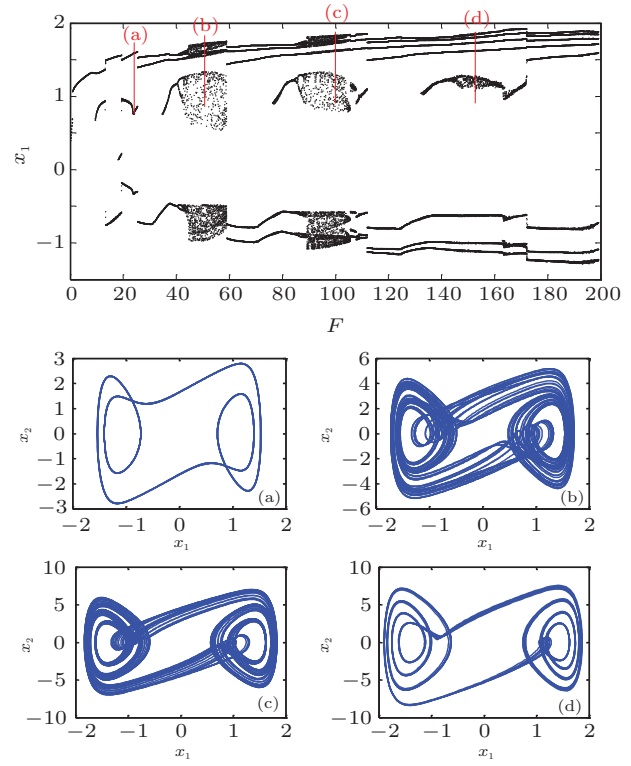


Fig. 12. (color online) Bifurcation diagram of the order of 0.95 when $n = 9$.

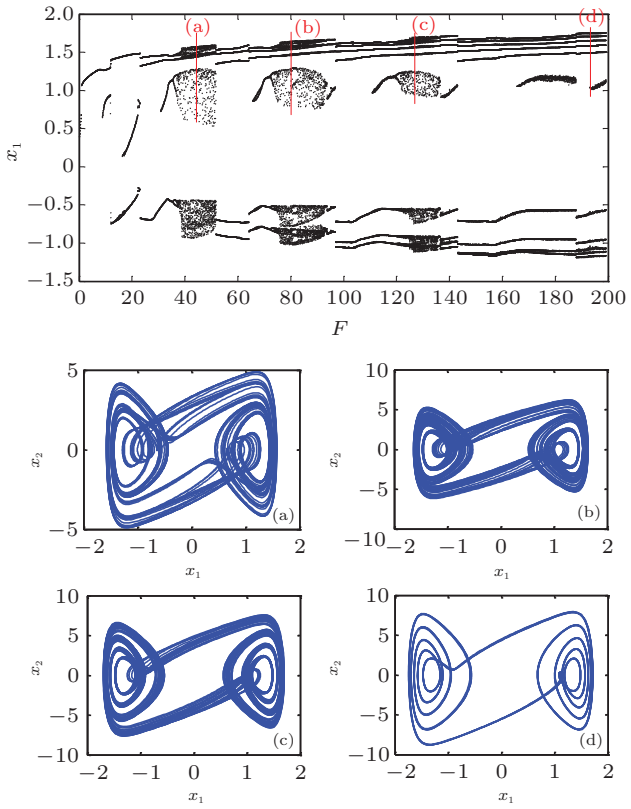


Fig. 13. (color online) Bifurcation diagram of the order of 0.95 when $n = 11$.

When the parameter n is further increased, there are intermittent chaotic regions as shown in the bifurcation diagrams Figs. 11, 12, and 13. Further more, when the fractional-order iron core transformer model is in chaotic status, the harmonic components show the same characteristic as the integer-order one. When the system becomes periodic, the frequency doubling components appeared as shown in Fig. 14.

Set $n = 7$ as an example, the period-doubling bifurcations can satisfy the Feigenbaum constant. The first period-doubling is in $F = 10.45$, and the system comes into period two. The second period-doubling is $F = 41.95$, and the third one is $F = 48.696$. The Feigenbaum constant is

$$\delta = \frac{\alpha_n - \alpha_{n-1}}{\alpha_{n+1} - \alpha_n} = \frac{41.95 - 10.45}{48.696 - 41.95} = 4.669. \tag{9}$$

As shown in Table 1, harmonic components in the fractional-order system are mostly odd. When $F = 65$, for the integer-order system, the principal component of harmonics is fundamental. For the fractional-order system, the principal component of harmonics is the 5th. Increase the external excitation F to 200, the main component of harmonic changes. For the integer-order system, since the system is in a chaotic state, harmonic components become complex. The principal harmonic component is a non-integer multiple of the fundamental. For the fractional-order system, the component of the harmonic is still an integral multiple of the fundamental and the principal component of harmonics is the 11th. The above analysis shows that the small change of order not only affects the dynamic behavior of the system, but also significantly affects the harmonic components of the system.

3. Implementation of the fractional-order ferroresonance system based on nonlinear circuit emulator

Since the nonlinear inductance of arbitrary order is difficult to be obtained in practical engineering, the author verifies the correctness of the theoretical analysis of the fractional-order ferroresonance system with the method of analog circuit based on the mathematical model of the system indirectly. As is known, the method we used in numerical simulation cannot be implementation in circuit. The solving precision of the predictor–corrector method and the frequency domain method is different, which is reported in Ref. [36].

The fractional integral operator of order "q" can be represented by the transfer function $F(s) = 1/s^q$ in the frequency domain. In Ref. [34], an effective algorithm is developed to approximate the fractional-order transfer functions. The approximation of $1/s^{0.95}$ with error of approximately 1 dB is given by

$$H(s) = \frac{1}{s^{0.95}} = \frac{1.2831s^2 + 18.6004s + 2.0833}{s^3 + 18.4738s^2 + 2.657s + 0.003}. \tag{10}$$

The chain structure of the fractance is shown in Fig. 15. $H(s)$ can be expressed as

$$H(s) = \frac{1/C_2}{s + 1/(R_{21}C_2)} + \frac{1/C_3}{s + 1/(R_{22}C_3)} + \frac{1/C_4}{s + 1/(R_{23}C_4)} \tag{11}$$

Comparing Eqs. (13) and (14), the following parameters can be obtained: $R_{21} = 1.7$ kΩ, $R_{22} = 171.7$ kΩ, $R_{23} = 79.2392$ MΩ, $C_2 = 3.1816$ μF, $C_3 = 4.0510$ μF, $C_4 = 1.1175$ μF, $R_{24} = 1.7$ kΩ, $R_{25} = 171.7$ kΩ, $R_{26} = 79.2392$ MΩ, $C_5 = 3.1816$ μF, $C_6 = 4.0510$ μF, $C_7 = 1.1175$ μF.

The fractional-order ferroresonance system is implemented by Orcad/Pspice. In the analog circuit, which is shown in Fig. 16, parameters are taken as follows: $R_1 = R_2 = R_4 = R_5 = R_7 = R_{12} = R_{13} = R_{16} = R_{17} = R_{19} = R_{20} = 1$ kΩ, $R_3 = 10$ kΩ, $R_6 = R_9 = 2.6$ kΩ, $R_8 = 100$ Ω, $R_{10} = 650$ Ω, $C_1 = 100$ μF.

Nonlinear terms of this fractional-order ferroresonance are implemented by analog multiplier AD633. The circuit is consists of resistors and multipliers, parameters are $R_{27} = R_{29} = R_{31} = R_{33} = R_{34} = 1$ kΩ, $R_{28} = R_{30} = R_{32} = 10$ kΩ.

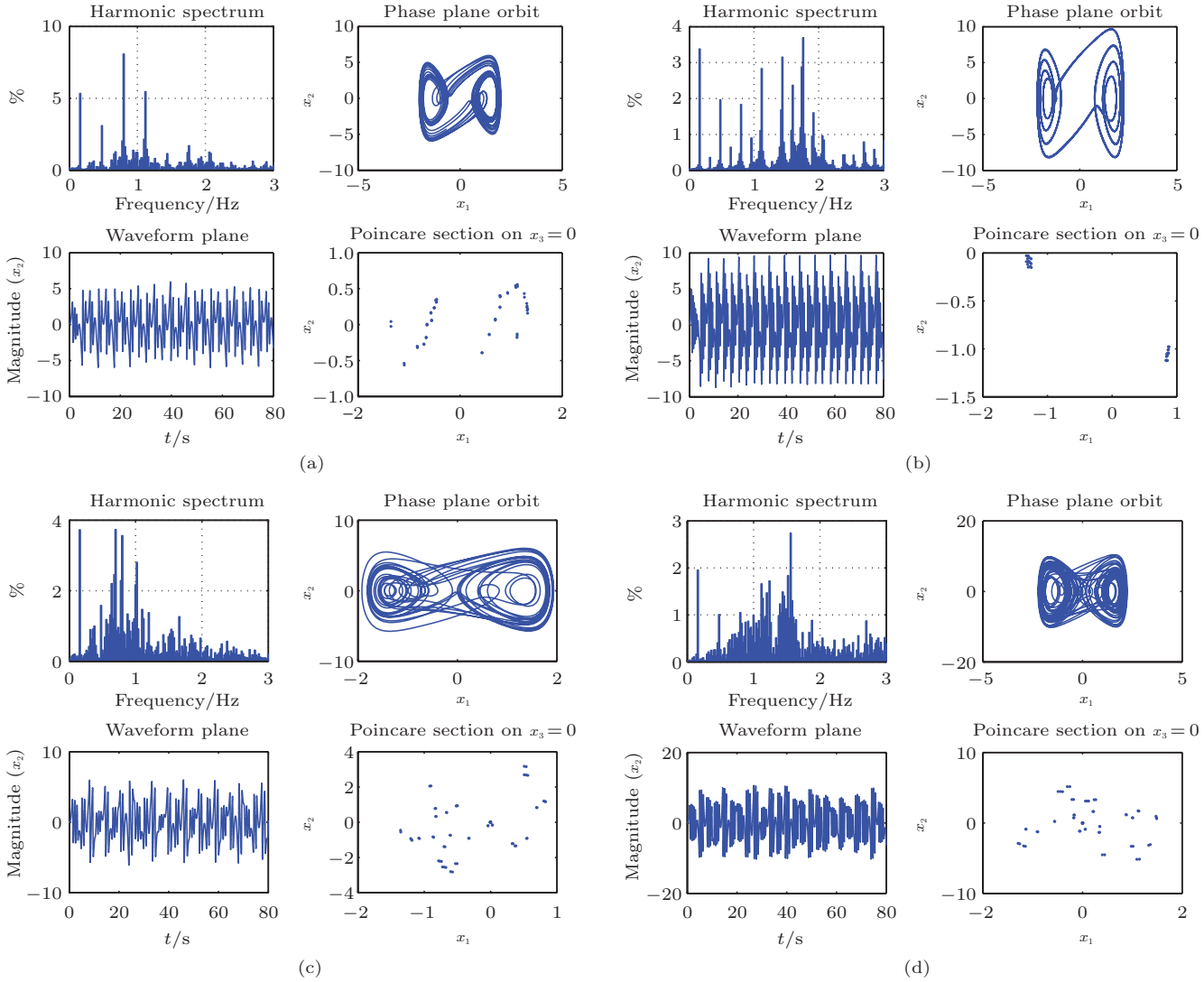


Fig. 14. (color online) Harmonic components of iron core transformer in order of 0.95. (a) Fractional-order system for $F = 65$. (b) Fractional-order system for $F = 200$. (c) Integer-order system for $F = 65$. (d) Integer-order system for $F = 200$.

Table 1. Harmonic components when $n = 7$.

Range	1st/Hz	2nd/Hz	3rd/Hz	4th/Hz
$q = 1, F = 65$	0.6997	0.1592 (fundamental)	0.796 (5th)	1.0196
$q = 0.95, F = 65$	0.796 (5th)	1.1144 (7th)	0.1592	0.4776 (3rd)
$q = 1, F = 200$	1.5594	0.1592	1.519	1.2393
$q = 0.95, F = 200$	1.7512 (11th)	0.1592	1.4328 (9th)	1.1144 (7th)

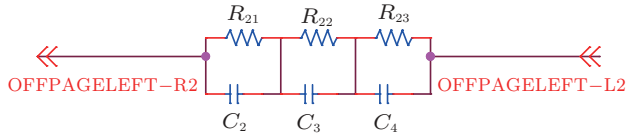


Fig. 15. (color online) Integration circuit for the fractional order 0.95.

The chaotic attractor can be obtained by analog circuit. As shown in Figs. 18 and 19, for $n = 7, F = 200$, the fractional-order system is in periodic state, but the integer-order system is in chaotic state. The results of harmonic analysis and numerical simulation are basically the same, which verifies the correctness of the theoretical analysis.

4. Chaotic synchronization based on fractional-order adaptive sliding mode control method

4.1. Fractional-order adaptive sliding mode control strategy

In this paper, to eliminate the abnormal operation state of power system caused by ferromagnetic chaos, the fractional-order adaptive sliding mode control (FASMC) is proposed. The design of the FASMC consists of two main steps: selection of an appropriate sliding surface and definition of a control law.

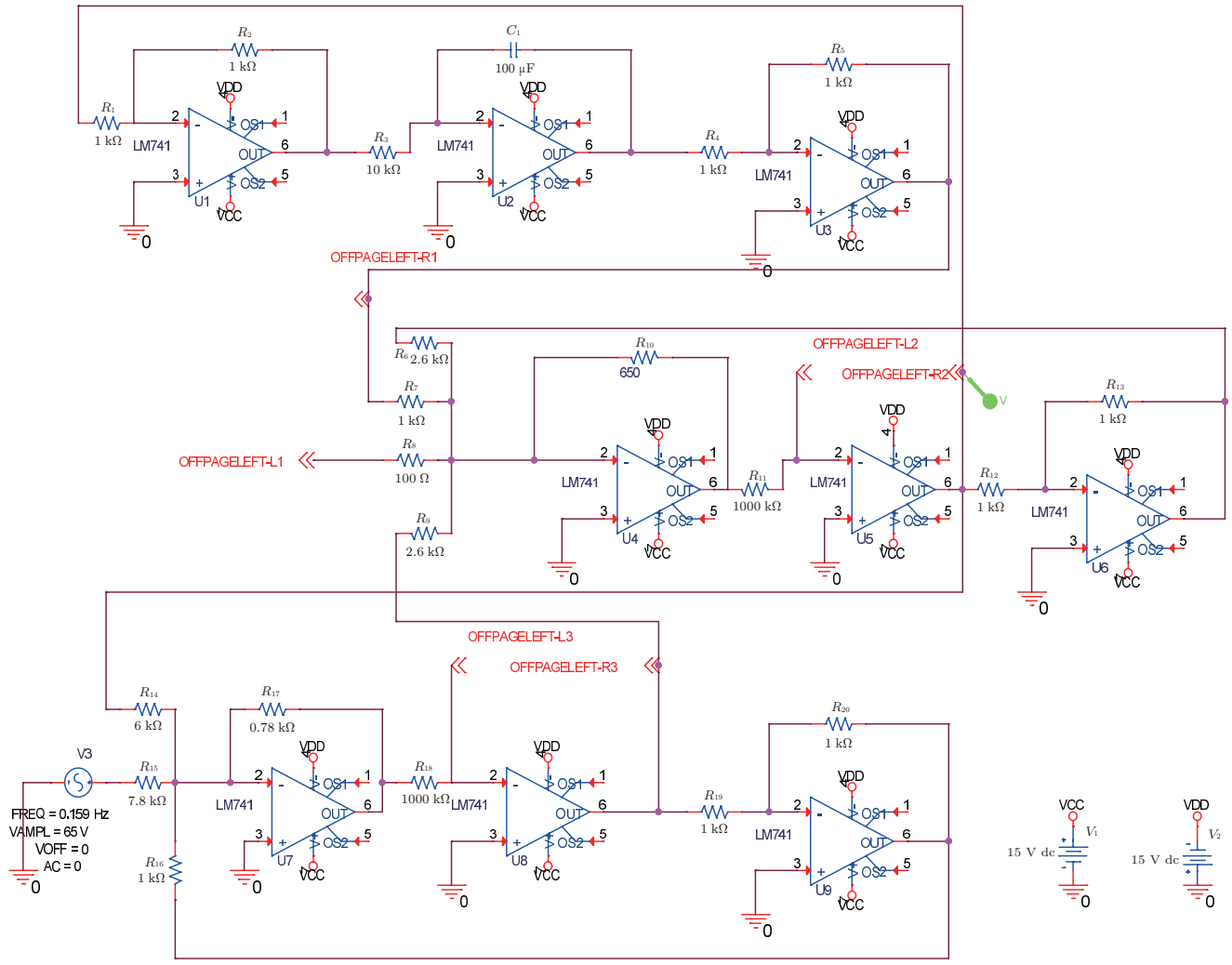


Fig. 16. (color online) Simulator circuit of fractional-order ferroresonance system.

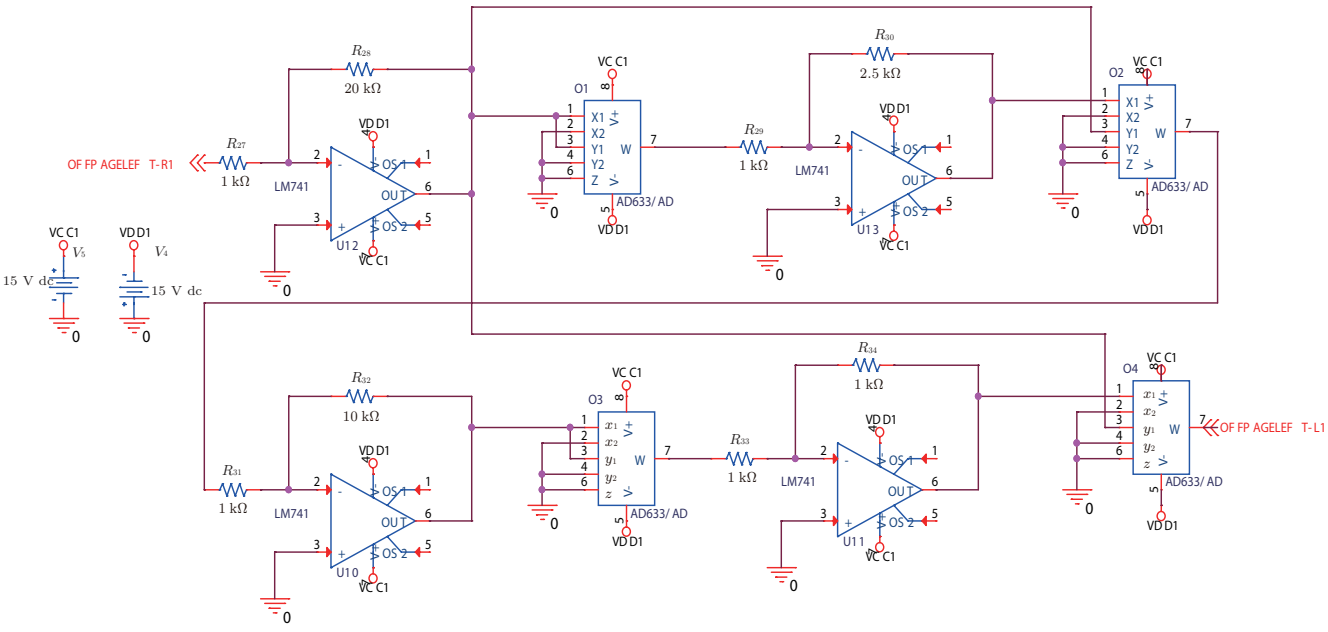


Fig. 17. (color online) Circuit realization of nonlinear inductance model.

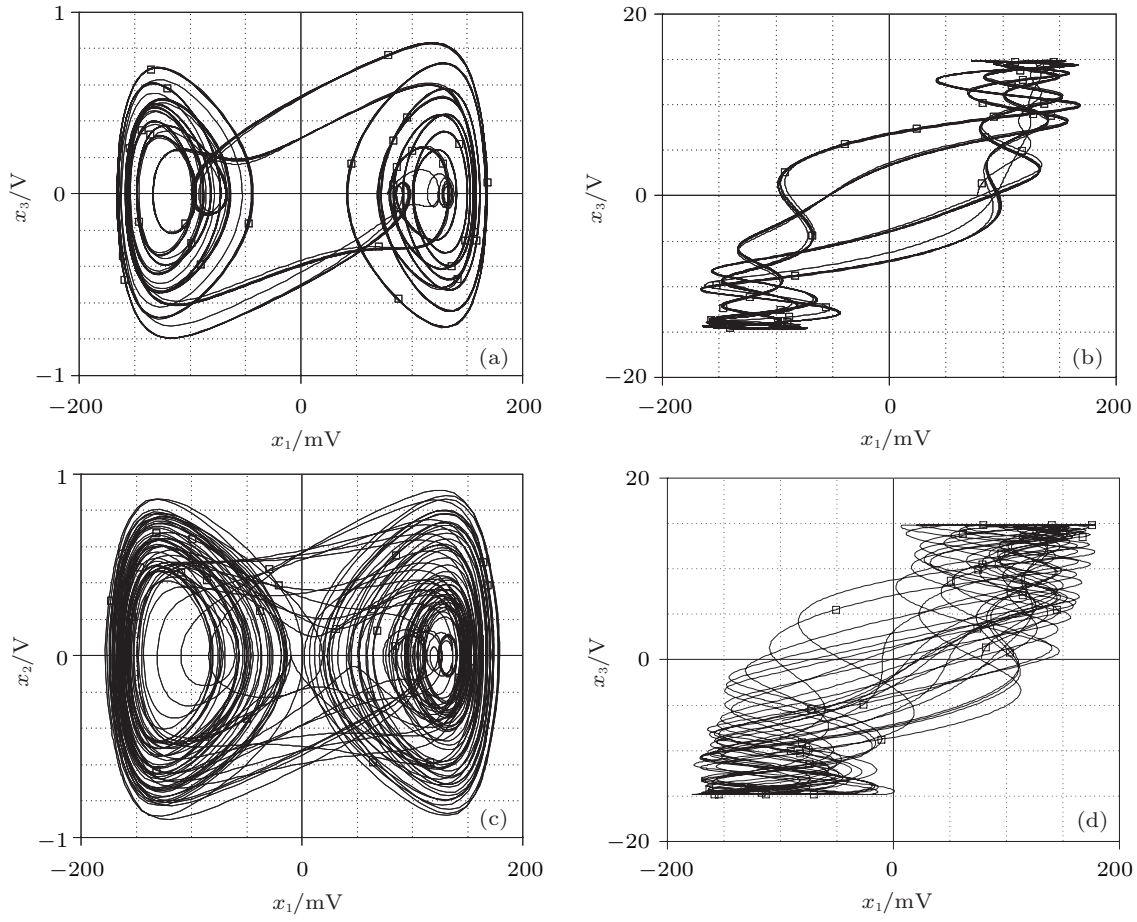


Fig. 18. Attractors of ferroresonance system for $n = 7$, $F = 200$. (a) Fractional-order system ($q = 0.95$) x_1–x_2, (b) fractional-order system ($q = 0.95$) x_1–x_3, (c) integer-order system x_1–x_2, (d) integer-order system x_1–x_3.

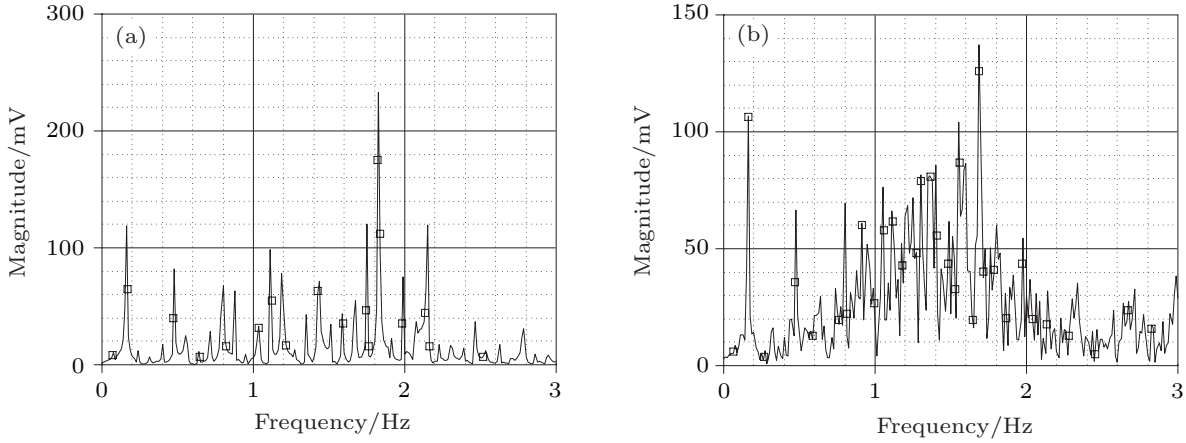


Fig. 19. Harmonic components of ferroresonance system for $n = 7$, $F = 200$. (a) Fractional-order system ($q = 0.95$), (b) integer-order system.

Consider the drive system

$$D^q x = Ax + f(x), \tag{12}$$

and the response system:

$$D^q y = By + g(y) + U, \tag{13}$$

where $x, y \in R^{n\times n}$ are state variables of driving system and response system. $f(x)$, $g(y)$ are the nonlinear part. The erroneous dynamical fractional-order system between the drive system (12) and response system (13) can be expressed as

$$D^q e = By + g(y) - Ax - f(x) + U. \tag{14}$$

A fractional-order sliding surface is proposed:

$$s_i(t) = a_i D^{q-1} e_i(t) + \int_0^t \operatorname{sgn}(e_i(\tau))\,|e_i(\tau)|^{\alpha} \mathrm{d}\tau, \tag{15}$$

where $s_i(t) \in R$ and $0 < \alpha < 1$ and $a_i > 0$, $i = 1, 2, \ldots, n$, let $a_i = 1$. For the existence of the sliding mode it is necessary

and sufficient that

$$s_i(t) = D^{q-1}e_i(t) + \int_0^t \operatorname{sgn}(e_i(\tau))\,|e_i(\tau)|^{\alpha}\mathrm{d}\tau, \quad (16)$$

$$\dot{s}_i(t) = D^{q}e_i(t) + \operatorname{sgn}(e_i(t))\,|e_i(t)|^{\alpha} = 0. \quad (17)$$

In order to increase the robustness and performance of the system, the adaptive law are defined as

$$\dot{K}_i = \theta \sum_{j=1}^{n} |e_j|\,|s_i|, \quad \theta > 0. \quad (18)$$

Adaptive coefficient θ is used to adjust the adaptive law.

Theorem 1 In order to stabilize the error system, the following fractional-order controller is designed

$$\begin{aligned} U(t) \;=\; & -Bx - g(y) + Ax + f(x) \\ & - \operatorname{sgn}(e_i)\,|e_i|^{\alpha} - \mu K_i \sum_{i=1}^{n} |e_i| \operatorname{sgn}(s_i). \end{aligned} \quad (19)$$

It always satisfies the reaching condition, that means the error system under arbitrary initial conditions will reach the sliding surface $S = 0$.

Proof Choose a positive–definite function in form of

$$V(t) = \frac{1}{2}\sum_{i=1}^{n} s_i^2 + \frac{1}{2\theta}\sum_{i=1}^{n} \mu (K_i - K^*)^2, \quad (20)$$

where $K^* > M/\mu$

$$\begin{aligned} & \dot{V}(t) \\ = & \sum_{i=1}^{n} s_i \dot{s}_i + \frac{1}{\theta}\mu \sum_{i=1}^{n} (K_i - K^*)\dot{K}_i \\ = & \sum_{i=1}^{n} s_i \left(D^q e_i(t) + \operatorname{sgn}(e_i(t))\,|e_i(t)|^{\alpha}\right) \\ & + \frac{1}{\theta}\mu \sum_{i=1}^{n} (K_i - K^*)\theta \left(\sum_{i=1}^{n} |e_j|\right)|s_i| \\ = & \sum_{i=1}^{n} s_i \Bigg(Be_i(t) - \operatorname{sgn}(e_i(t))\,|e_i(t)|^{\alpha} \\ & - \mu K_i \sum_{j=1}^{n} |e_j(t)|\, sgn(s_i(t)) \Bigg) \\ & + \sum_{i=1}^{n} s_i \left(\operatorname{sgn}(e_i(t))\,|e_i(t)|^{\alpha}\right) \\ & + \mu \sum_{i=1}^{n} K_i \left(\sum_{i=1}^{n} |e_j|\right)|s_i| - \mu \sum_{i=1}^{n} K^* \left(\sum_{i=1}^{n} |e_j|\right)|s_i| \\ = & \left(-\mu \sum_{i=1}^{n} s_i sgn(s_i) \left(K_i \sum_{j=1}^{n} |e_j|\right)\right. \\ & \left. + \mu \sum_{i=1}^{n} |s_i| \left(K_i \sum_{i=1}^{n} |e_j|\right)\right) \\ & + \left(\sum_{i=1}^{n} s_i \left(-sgn(e_i(t))\,|e_i(t)|^{\alpha}\right)\right. \\ & \left. + \sum_{i=1}^{n} s_i \left(\operatorname{sgn}(e_i(t))\,|e_i(t)|^{\alpha}\right)\right) \\ & + \left(\sum_{i=1}^{n} s_i \left(Be_i(t)\right) - \mu \sum_{i=1}^{n} K^* \left(\sum_{i=1}^{n} |e_j|\right)|s_i|\right). \end{aligned} \quad (21)$$

Since the coefficient matrix B can be written as $\|B\| = \sum_{i=1}^{n}\sum_{j=1}^{n} b_{ij}$, M can be simply obtained, which satisfies $0 \le \|B\| \le M$

$$\begin{aligned} & \dot{V}(t) \\ \le & \sum_{i=1}^{n} |s_i| \cdot \left(\sum_{i=1}^{n}\sum_{j=1}^{n} |b_{ij}| \cdot |e_j|\right) - \mu K^* \sum_{i=1}^{n}\sum_{j=1}^{n} |e_j|\,|s_i| \\ \le & \sum_{i=1}^{n} |s_i| \cdot \left(\sum_{i=1}^{n}\sum_{j=1}^{n} |b_{ij}|\right) \cdot \left(\sum_{j=1}^{n} |e_j|\right) \\ & - \mu K^* \sum_{i=1}^{n}\sum_{j=1}^{n} |e_j|\,|s_i|, \end{aligned} \quad (22)$$

$$\begin{aligned} & \sum_{i=1}^{n} |s_i| \cdot \left(\sum_{i=1}^{n}\sum_{j=1}^{n} |b_{ij}|\right) \cdot \left(\sum_{j=1}^{n} |e_j|\right) \\ & - \mu K^* \sum_{i=1}^{n}\sum_{j=1}^{n} |e_j|\,|s_i| \\ = & \|B\| \sum_{i=1}^{n} |s_i| \cdot \sum_{j=1}^{n} |e_j| - \mu K^* \sum_{i=1}^{n}\sum_{j=1}^{n} |e_j|\,|s_i| \\ \le & M \sum_{i=1}^{n}\sum_{j=1}^{n} |e_j|\,|s_i| - \mu K^* \sum_{i=1}^{n}\sum_{j=1}^{n} |e_j|\,|s_i| \\ = & -(\mu K^* - M) \sum_{i=1}^{n}\sum_{j=1}^{n} |e_j|\,|s_i|. \end{aligned} \quad (23)$$

It is obvious that the condition $\dot{V}(t) < 0$ will be satisfied, and the trajectories of the error system will converge to the sliding surface. In summary, the drive system and the response system can achieve synchronization.

4.2. Numerical simulation

Considering parameters of drive and response systems are $q = 0.95, n = 7$. The drive system is

$$\begin{aligned} \frac{\mathrm{d}x_1}{\mathrm{d}\tau} &= x_1, \\ \frac{\mathrm{d}^{0.95}x_2}{\mathrm{d}\tau^{0.95}} &= 0.25(x_2 - x_1) - 6.5x_1, \\ \frac{\mathrm{d}^{0.95}x_3}{\mathrm{d}\tau^{0.95}} &= 0.13x_2 - 0.78x_3 + 65\sin\tau. \end{aligned} \quad (24)$$

The response system is described by

$$\begin{aligned} \frac{\mathrm{d}y_1}{\mathrm{d}\tau} &= y_1 + U_1, \\ \frac{\mathrm{d}^{0.95}y_2}{\mathrm{d}\tau^{0.95}} &= 0.25(y_2 - y_1) - 0.65\left(y_1^7 + y_1\right) + U_2, \\ \frac{\mathrm{d}^{0.95}y_3}{\mathrm{d}\tau^{0.95}} &= 0.13y_2 - 0.78y_3 + 65\sin\tau + U_3. \end{aligned} \quad (25)$$

The change of parameters may significantly improve the performance of the FASMC.[37] As shown in Fig. 20(a), with

the increase of the gain θ in the adaptive law, the synchronization setup time decreases. In Fig. 20(b), the synchronisation setup time increases with α.

Parameters of the FASMC controller are: $\theta = 5$, $\alpha = 0.6$. Numerical simulation using SIMULINK proves that the conclusion mentioned in Section 4 is right. At $t = 20$ s, the controller u is added to the response system. Trajectories of the response system asymptotically approach of the drive system as shown in Figs. 21(a)–21(c) and erroneous vector eventually converges to zero, as shown in Fig. 21(d). Simulation results indicate that the synchronisation of two fractional-order ferroresonance systems is realized.

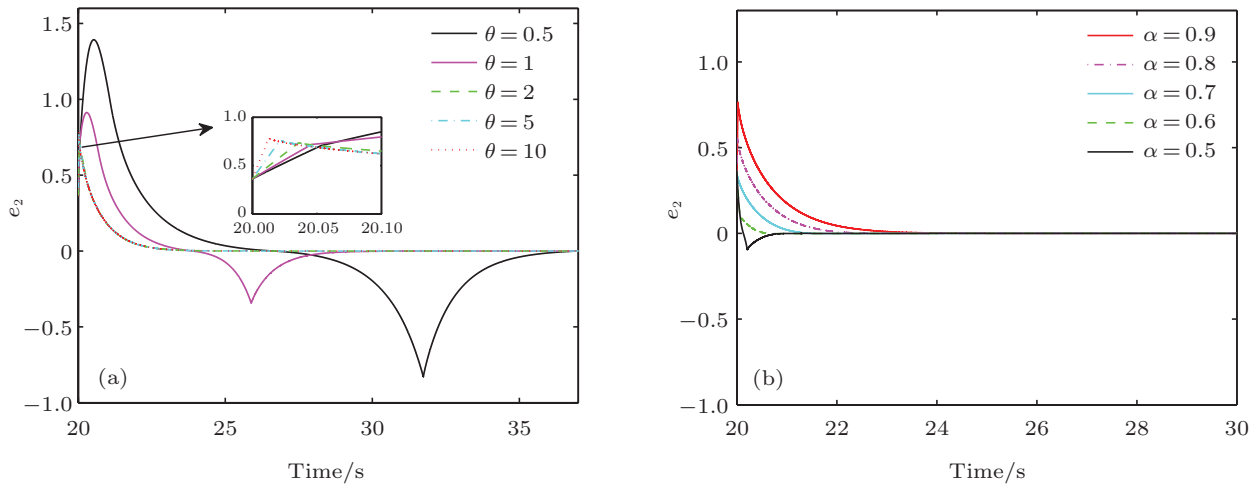


Fig. 20. (color online) Synchronization setup time with different parameters: (a) parameter θ, (b) parameter α.

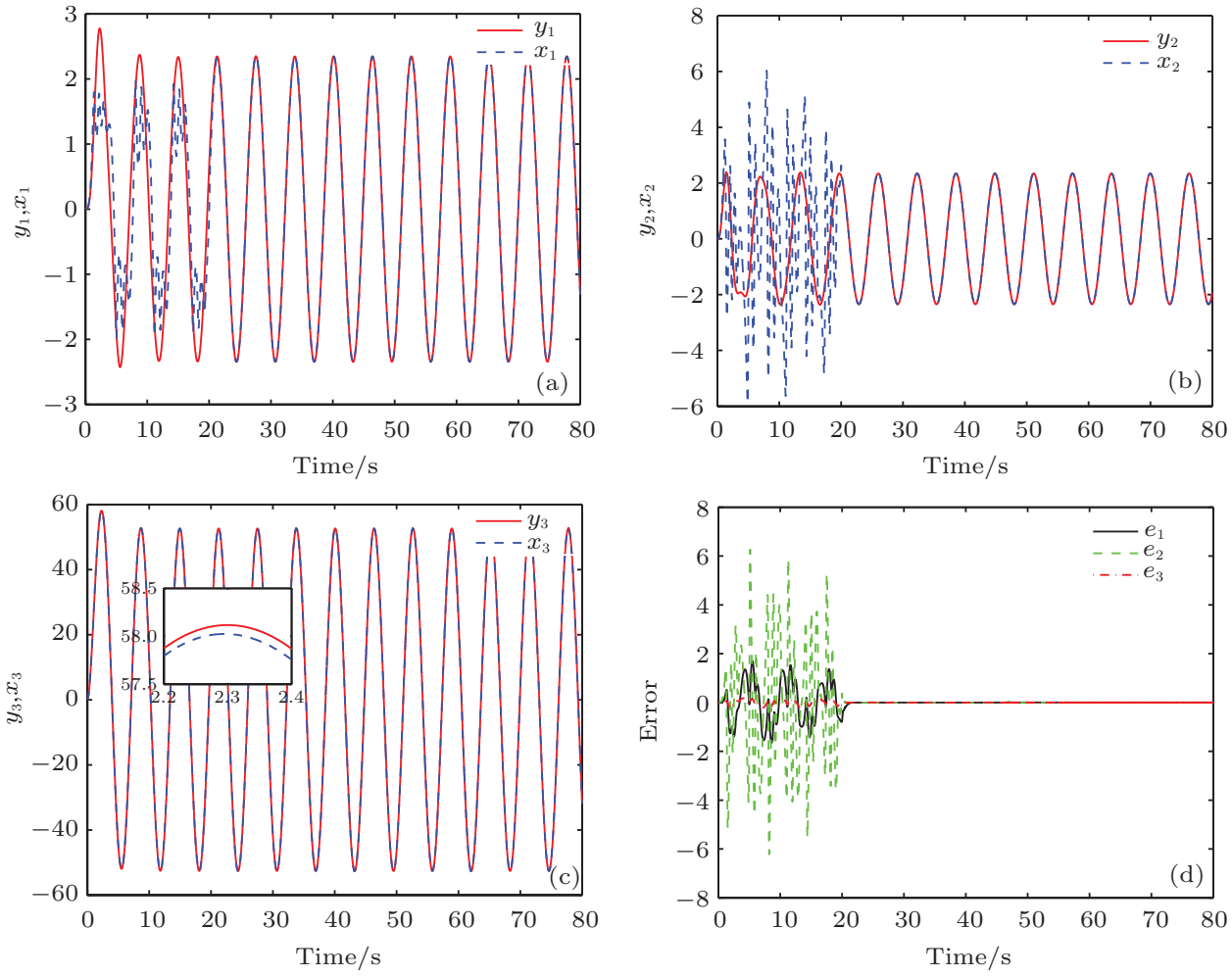


Fig. 21. (color online) Synchronization between two fractional-order ferroresonance systems. (a) Time waveforms of the states x_1 (dashed) and y_1 (solid); (b) Time waveforms of the states x_2 (dashed) and y_2 (solid); (c) Time waveforms of the states x_3 (dashed) and y_3 (solid); (d) Error dynamical system states e_1, e_2, e_3.

5. Conclusions

In this paper, fractional calculus is introduced into the modeling of the ferroresonance system based on fractional-order characteristics of the capacitance. The influence of the order on the dynamic behavior of ferroresonance system is studied. Compared with the integral-order ferroresonance system, the small change of the order not only affects the dynamic behavior of the system, but also significantly affects the harmonic components of the system. In order to eliminate the abnormal operation state of the power system caused by ferromagnetic chaos, a fractional-order adaptive sliding mode control method is used to realize the synchronization of this fractional-order system. Since the introduction of the fractional-order sliding mode surface and the adaptive factor, the robustness and disturbance rejection of the controlled system are enhanced. The circuit and numerical simulation results demonstrated that the correctness of the analysis of the fractional-order ferroresonance system model and the proposed FASMC controller works well for suppression of the ferroresonance over voltage.

References

[1] Dancaa M F, Tang W K S and Chen G R 2016 *Chaos, Solitons and Fractals* **84** 31
[2] Podlubny I 1999 *Fractional Differential Equations* p. 261.
[3] Radwan A G and Fouda M E 2013 *Circ. Syst. Signal Process.* **5** 32
[4] Podlubny I 1998 *System Structure and Control* **1–2** 215
[5] Jonscher A K 1999 *J. Phys. D: Appl. Phys.* **14** 32:R57
[6] Westerlund S and Ekstam L 1994 *IEEE Trans. Dielectr. Electr. Insul.* **1** 826
[7] Jesus I S and Machado J A T 2009 *Nonlinear Dyn.* **56** 45
[8] Haba T C, Ablart G, Camps T and Olivie F 2005 *Chaos, Solitons and Fractals* **24** 479
[9] Petras I 2008 *Chaos, Solitons and Fractals* **38** 140
[10] Adolfsson K, Enelund M and Olsson P 2005 *Mech. Time-Depend. Mat.* **9** 15
[11] Ahmed E and Elgazzar A S 2007 *Physica A* **379** 607
[12] Pahnehkolaei S M A, Alfi A and Machado J A T 2017 *Commun. Nonlinear Sci. Numer. Simul.* **47** 328
[13] Yang N N, Liu C X and Wu C J 2012 *Chin. Phys. B* **21** 080503
[14] Yang N N, Wu C J, Jia R, *et al.* 2016 *Math. Problems in Engineering* **1** 1
[15] Moreles M A and Lainez R 2016 *Commun. Nonlinear Sci. Numer. Simul.* **46** 81
[16] Dzielinski A and Sierociuk D 2008 *Acta Montan Slovaca* **13** 136
[17] Hong Z, Qian J, Chen Di-Yi and Herbert H C Iu 2015 *Chin. Phys. B* **24** 080204
[18] Abu Bakar A, Khan, S A, Kwang T C and Abd Rahim N 2015 *IEEE J. T. Electr. Electr.* **10** 28
[19] Ribas J C L, Lourenco E M, Leite J V and Batistela N J 2013 *IEEE T. Magn.* **49** 1797
[20] Liu C X, Zhai D Q, Dong Z H and Liu Y 2010 *Acta Phys. Sin.* **59** 3733 (in Chinese)
[21] Simha V and Lee W J 2008 *IEEE Ind. Appl. Mag.* **14** 53
[22] Radmanesh H and Gharehpetian G B 2013 *Int. J. Elec. Power* **45** 1
[23] Oustaloup, A, Mreau X and Nouillant M 1996 *Control Eng. Pract.* **4** 1101
[24] Podlubny I 2003 *Fractional-Order Systems and Fractional-Order Controllers* pp. 43–54
[25] Wang D F, Zhang J Y and Wang X Y 2013 *Chin. Phys. B* **22** 040507
[26] Khanzadeh A and Pourgholi M 2016 *Nonlinear Dyn.* **86** 543
[27] Pooseh S, Almeida R and Torres D F M 2014 *J. Ind. Manag. Optim.* **10** 363
[28] Lin D and Wang X Y 2011 *Nonlinear Dyn.* **66** 89
[29] Aghababa M P, Khanmohammadi S and Alizadeh G 2011 *Appl. Math. Model.* **35** 3080
[30] Chen Y Q, Wei Y H, Zhong H and Wang Y 2016 *Nonlinear Dyn.* **85** 633
[31] Yin C, Chen Y Q and Zhong S M 2014 *IFAC Proceedings Volumes* **47** 5369
[32] Chen D Y, Zhang R F, Ma X Y and Wang J 2012 *Chin. Phys. B* **21** 120507
[33] Jesus I S and Machado J A T 2009 *Nonlinear Dyn.* **56** 45
[34] Wu C J, Zhang Y B and Yang N N 2011 *Chin. Phys. B* **20** 060505
[35] Diethelm K 2011 *Fract. Calc. Appl. Anal.* **14** 475
[36] He S B, Sun K H and Wang H H 2014 *Acta Phys. Sin.* **63** 030502 (in Chinese)
[37] He S B, Sun K H and Wang H H 2016 *The European Physical Journal Special Topics* **225** 97